

# Lamb shift in $\text{He}^+$ : Resolution of a discrepancy between theory and experiment

A. van Wijngaarden, F. Holuj, and G. W. F. Drake

*Department of Physics, University of Windsor, Windsor, Ontario, Canada N9B 3P4*

(Received 29 May 2000; published 5 December 2000)

An earlier measurement of the  $2^2S_{1/2}-2^2P_{1/2}$  Lamb shift in  $\text{He}^+$  by the anisotropy method is repeated in order to either verify or remove a significant discrepancy between theory and experiment. The principal change from our previous measurement is a redesigned photon detection system to eliminate a residual polarization sensitivity of the photon detectors. The result of the measurement corresponds to a Lamb shift of 14 041.13(17) MHz, in excellent agreement with the theoretical value 14 041.18(13) MHz. The good agreement between theory and experiment provides a clear test of the recently calculated two-loop binding correction of  $-1.339$  MHz.

DOI: 10.1103/PhysRevA.63.012505

PACS number(s): 31.30.Jv, 31.30.Gs

## I. INTRODUCTION

The  $2^2S_{1/2}-2^2P_{1/2}$  Lamb shift in  $\text{He}^+$  provides an important supplement to measurements of the corresponding classic Lamb shift in hydrogen for two reasons. First, the higher-order binding corrections increase rapidly with nuclear charge, and so are much larger in  $\text{He}^+$  than in H. For example, the large two-loop binding correction to the electron self-energy recently calculated by Pachucki [1] and Eides and Shelyuto [2] scales with nuclear charge as  $Z^5$ , giving a contribution of  $-1.339$  MHz in  $\text{He}^+$  as compared with  $-0.0418$  MHz in H. Second, the interpretation of Lamb shift measurements in H is obscured by uncertainties in the proton size, resulting in an uncertainty in the calculated Lamb shift that is as large as the two-loop binding correction. In contrast, the nuclear radius uncertainty is relatively much less in  $\text{He}^+$ , so that a sufficiently accurate measurement provides a clear test of the two-loop binding correction.

In a previous paper [3] we reported a measurement of the Lamb shift in  $\text{He}^+$ , using the anisotropy method. The measurement is nominally accurate enough to be sensitive to the two-loop binding correction, but the result of 14 042.52(16) MHz lies several standard deviations above the theoretical value of 14 041.18(13) MHz (see Table I) when the two-loop binding correction is included. In order to resolve the discrepancy, we first performed a parallel high-precision measurement of the Lamb shift in H [4]. The result of 1057.852(15) MHz verifies that the anisotropy method yields results for hydrogen that are in agreement with direct microwave resonance measurements and with theory. The present paper reports the results of another anisotropy measurement of the Lamb shift in  $\text{He}^+$ . The principal change from our previous measurement is a redesigned system for photon detection. The change was required in order to eliminate a residual polarization sensitivity present in our earlier measurement. The polarization sensitivity introduced a source of systematic error which has now been corrected.

The anisotropy method of measuring Lamb shifts has undergone a progressive series of refinements [5–9] since it was first proposed by Drake and Grimley [10]. Its principal advantage over direct measurements of the transition frequency is that it is not limited in accuracy by the large level width of the  $2p$  state. The directly measured quantity is the ratio of total photon fluxes emitted parallel and perpendicular

to an electrostatic quenching field, integrated over frequencies. Closely related measurements with the same apparatus have been used to measure the level width of the  $2p$  state [11] and the relativistic magnetic dipole matrix element for the  $2s \rightarrow 1s$  transition [12].

In Sec. II, the theoretical contributions to the Lamb shift are summarized, and the known scalings of each term with  $Z$  and nuclear mass are used to calculate updated values for the Lamb shift and fine structure splitting in  $\text{He}^+$ . Section III briefly reviews the theoretical aspects of the anisotropy method. The technical approach together with a detailed description of the redesigned photon detectors are described in Sec. IV. The results are presented in Sec. V, followed by a comparison with theory and discussion in Secs. VI and VII.

## II. LAMB SHIFT THEORY

The states  $2^2S_{1/2}$  and  $2^2P_{1/2}$  are degenerate according to the solutions to the Dirac equation for a single electron moving in the Coulomb field of the nucleus. This degeneracy is lifted by the quantum electrodynamic (QED) effects of vacuum polarization and electron self-energy, as well as by the finite size of the nucleus. This section first discusses the QED terms and then the finite nuclear size correction.

### A. QED contributions

The nonrelativistic theory of the QED effects results in a double expansion in powers of  $\alpha$  and  $Z\alpha$ , where  $\alpha$  is the fine structure constant. In lowest order, the QED shift for an electron with quantum numbers  $n$ ,  $l$ , and  $j$  is given by the well-known expression

$$\begin{aligned} \Delta E_{\text{QED}} = & \frac{4\alpha(Z\alpha)^4 mc^2}{3\pi n^3} \left\{ \left[ \frac{19}{30} + \ln(Z\alpha)^{-2} \right] \delta_{l,0} - \beta_{n,l} \right. \\ & + \frac{3}{8} (1 - \delta_{l,0}) c_{l,j} / (2l+1) + O(Z\alpha) + O(\alpha/\pi) \\ & \left. + O(m/M) \right\}, \end{aligned} \quad (1)$$

where  $c_{l,j} = 2(j-l)/(j+\frac{1}{2})$  is the anomalous magnetic moment factor, and  $\beta_{n,l}$  denotes the Bethe logarithm. The numerical values for  $n=2$  are [13]

$$\beta_{2s} = 2.811\,769\,893\,120, \quad \beta_{2p} = -0.030\,016\,708\,630.$$

TABLE I. Contributions to the energies of the  $n=2$  states of  $\text{He}^+$ . Each entry includes reduced mass corrections. The values of the fundamental constants are  $R_\infty=10\,973\,731.568\,516(84)\text{ m}^{-1}$ ,  $\alpha^{-1}=137.035\,999\,58(52)$ , and  $M/m=7294.299\,508(16)$  for the  $\alpha$  particle to electron mass ratio. Units are MHz.

Contribution ( $\alpha mc^2$ )	$2^2S_{1/2}$	$2^2P_{1/2}$	$2^2P_{3/2}$
$(Z\alpha)^4 \ln(Z\alpha)^{-2}$	18 340.595	0.000	0.000
$(Z\alpha)^4$	-4 725.621	-206.095	200.725
$\alpha(Z\alpha)^4$	2.037	0.414	-0.207
$\alpha^2(Z\alpha)^4$	0.004	-0.003	0.002
$(Z\alpha)^4$ muonic pol.	-0.010	0.000	0.000
$(Z\alpha)^4$ hadronic pol.	-0.006	0.000	0.000
$(Z\alpha)^5$	228.402	0.000	0.000
$\alpha(Z\alpha)^5$ (one loop)	0.061	0.000	0.000
$\alpha(Z\alpha)^5$ (two-loop VP)	0.088	0.000	0.000
$\alpha(Z\alpha)^5$ (two-loop SE)	-1.339	0.000	0.000
$(Z\alpha)^6 \ln^2(Z\alpha)^{-2}$	-7.396	0.000	0.000
$(Z\alpha)^6 \ln(Z\alpha)^{-2}$	-0.391	1.677	0.944
$(Z\alpha)^6 G_{\text{SE}}(Z\alpha)$	-10.620(9)	-0.330(3)	-0.165(3)
$(Z\alpha)^6 G_{\text{VP}}(Z\alpha)$	-0.276	-0.022	-0.005
$(Z\alpha)^6 G_{\text{WK}}(Z\alpha)$	0.019	0.000	0.000
$\alpha(Z\alpha)^6 \ln^3(Z\alpha)^{-2}$	-0.144	0.000	0.000
$\alpha(Z\alpha)^6 \ln^2(Z\alpha)^{-2}$	0.010(130) <sup>a</sup>	0.006	0.006
$\alpha(Z\alpha)^6 \ln(Z\alpha)^{-2}$	-0.003	0.000(3) <sup>a</sup>	0.000(3) <sup>a</sup>
Terms of order $\alpha(Z\alpha)^7$	0.000(15) <sup>a</sup>	0.000(15) <sup>a</sup>	0.000(15) <sup>a</sup>
$(Z\alpha)^5 m/M$	2.547	-0.138	-0.138
$(Z\alpha)^6 m/M$	-0.015	0.007	0.007
$(Z\alpha)^7 \ln^2(Z\alpha) m/M$	-0.001	0.000	0.000
$\alpha(Z\alpha)^5 m/M$	-0.035	0.000	0.000
$Z(Z\alpha)^5 (m/M)^2$	0.002	0.000	0.000
$\alpha(Z\alpha)^6 m/M$	0.002	0.000	0.000
Finite nuclear size	8.786(10)	0.000	0.000
Subtotal	13 836.697(130)	-204.485(15)	201.170(15)
Dirac fine structure	0.000	0.000	175 187.848
Total	13 836.697(130)	-204.485(15)	175 389.018(15)
$E(2^2S_{1/2}) - E(2^2P_{1/2})$	14 041.18(13)		
$E(2^2P_{3/2}) - E(2^2P_{1/2})$	175 593.50(2)		

<sup>a</sup>Uncertainties due to uncalculated terms.

A great deal of effort by a large number of authors has been devoted to the evaluation of the higher-order corrections to this expression, as recently reviewed in detail by Eides, Grotch, and Shelyuto [14] and by Mohr and Taylor [15]. These reviews focus primarily on the case of hydrogen, but, since the scaling of each term is known as a function of  $Z$  and  $m/M$ , the corresponding QED corrections for the case of  $\text{He}^+$  can be readily calculated. In Table I we have grouped together the 48 individual contributions to the QED shift contained in Tables II through IX of Ref. [14] according to their powers of  $\alpha$ ,  $Z\alpha$ , and  $\ln(Z\alpha)^{-2}$ . Each term contains a reduced mass scaling factor of  $(m_r/m)^3$ , except for the anomalous magnetic moment terms where the scaling factor is  $(m_r/m)^2$  and the Dirac fine structure where the scaling (to lowest order) is  $(m_r/m)$ . The other mass-dependent recoil and radiative recoil terms are listed separately.

In the conventional notation, the terms  $G_{\text{SE}}(Z\alpha)$ ,  $G_{\text{VP}}(Z\alpha)$ , and  $G_{\text{WK}}(Z\alpha)$  represent an estimate of the sum of

all higher-order terms in the  $Z\alpha$  expansion for the self-energy, vacuum polarization, and Wickman-Kroll terms obtained by an interpolation between accurate results in the limit  $Z \rightarrow 0$  [16,17] and nonperturbative all-orders calculations for  $Z \geq 5$  [18]. Our interpolations agree to well within

TABLE II. Input data to calculate  $R_0$  from the observed  $R$  value of Eq. (9) and deduce the Lamb shift.

Quantity	Value
$E(2p_{3/2}) - E(2p_{1/2})$	175 593.50(2) MHz
$\Gamma(2p)$	$1.596\,44 \times 10^9\text{ s}^{-1}$
$(\delta R/R_0)_{np}$	$-2.37 \times 10^{-5}$
$(\delta R/R_0)_{\text{rel}}$	$0.64 \times 10^{-5}$
$(\delta R/R_0)_{M2}$	$-6.54 \times 10^{-5}$
$R^{(2)}$	$5.846\,7 \times 10^{-4}\text{ (kV/cm)}^2$
$R^{(4)}$	$-3.80 \times 10^{-6}\text{ (kV/cm)}^4$

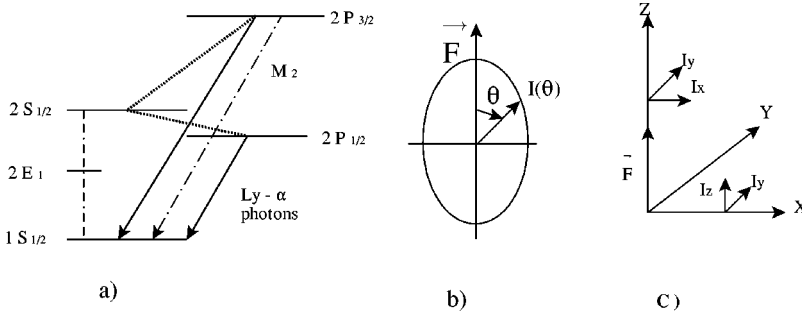


FIG. 1. (a) Electric field induced quenching of the metastable  $2^2S_{1/2}$  state in  $\text{He}^+$ . (b) Polar diagram for the intensity  $I(\theta)$  of the  $E1$  quench radiation emitted under the action of a static electric field  $F$ . The radiating system is at the origin. (c) The polarization of the quench radiation. Arrows alongside intensities indicate polarization vectors.

the uncertainties with those tabulated by Mohr [15,19]. The principal limitations on the accuracy are uncalculated terms of order  $\alpha(Z\alpha)^6 amc^2$  for the  $2^2S_{1/2}$  state, and terms of order  $\alpha(Z\alpha)^7 amc^2$  for the  $2^2P_j$  states.

Of particular interest in Table I is the relatively large contribution of  $-1.339$  MHz from the two-loop self-energy term of order  $\alpha(Z\alpha)^5 amc^2$ . This is the two-loop binding correction recently calculated by Pachucki [1] and Eides and Shelyuto [2]. It is an order of magnitude larger than the experimental uncertainty in our measurement.

### B. Finite nuclear size contribution

The finite nuclear size correction requires a more extended discussion. In the nonrelativistic limit, the correction is given by

$$\Delta E_{\text{ns}} = \frac{2\alpha^2 Z^4 mc^2}{3n^3} \left( \frac{r_{\text{rms}}}{a_0} \right)^2 \delta_{l,0}, \quad (2)$$

where  $r_{\text{rms}}$  is the rms nuclear radius for  $^4\text{He}$  and  $a_0$  is the Bohr radius. A very accurate value for  $r_{\text{rms}}$  can be inferred from measurements of the transition frequencies  $2s_{1/2}-2p_{1/2}$  and  $2s_{1/2}-2p_{3/2}$  in the muonic system  $\mu^- - \text{He}^{2+}$  [20], with the result  $r_{\text{rms}} = 1.673 \pm 0.001$  fm. However, the validity of this measurement has been questioned because of subsequent difficulties in observing the  $\mu^- - \text{He}^{2+}(2s)$  metastable state at high pressures [21–23]. Bracci and Zavattini [24] have argued that the observation of the muonic transition frequencies can be explained by the formation of  $\text{He}(\mu^- - \text{He}^{2+})$  triplet molecular ions, but the status of the original experiment still remains unclear.

Fortunately, the above value for  $r_{\text{rms}}$  is in excellent agreement with the value obtained from electron scattering measurements. The three measurements are in good agreement with each other and yield the combined result  $r_{\text{rms}} = 1.674 \pm 0.012$  fm [25]. The nuclear radius correction listed in Table I assumes the more accurate value  $r_{\text{rms}} = 1.673 \pm 0.001$  fm from the muonic helium measurement, and the calculated Lamb shift is  $14\,041.18 \pm 0.13$  MHz. If instead the electron scattering value for  $r_{\text{rms}}$  is used, then the calculated Lamb shift changes only slightly to  $14\,041.19 \pm 0.19$  MHz. In either case, the calculated fine structure splitting is  $\Delta_F = 175\,593.50 \pm 0.02$  MHz. The uncertainty of  $\pm 0.02$  MHz in  $\Delta_F$  has a negligible effect on the derivation of the Lamb shift from the anisotropy measurement.

## III. ANISOTROPY METHOD

A full account of the theory of quenching radiation asymmetries in hydrogenic ions has been given by Drake [26] and applications to the determination of the Lamb shift reviewed by van Wijngaarden *et al.* [3]. This section summarizes the main features of the method.

### A. Relation between Lamb shift and anisotropy

The anisotropy method for measuring the Lamb shift  $\mathcal{L} = E(2^2S_{1/2}) - E(2^2P_{1/2})$  for the  $n=2$  state in hydrogenic ions, as shown in Fig. 1(a), is based on the radiative decay modes of the  $2^2S_{1/2}$  state. We subject a fast ( $v/c \sim 10^{-2}$ ) beam of hydrogenic ions in the metastable  $2s$  state to a static electric field, perpendicular to the beam direction, as shown in Fig. 1(b) where the beam travels into the page, through the origin of the diagram. The dotted lines in Fig. 1(a) indicate the mixing of the  $2s_{1/2}$  state with the radiative  $2p_{1/2}$  and  $2p_{3/2}$  states by the field. This leads to field induced  $E1$  transitions to the ground state, together with  $M2$  transitions that proceed via the  $2p_{3/2}$  state, with emission of Ly  $\alpha$  photons. The Ly  $\alpha$  intensity for  $M2$  transitions is much weaker than for  $E1$  transitions.

Figure 1(b) is a polar diagram of the quench radiation intensity  $I(\theta)$  emitted at an angle  $\theta$  with respect to the electric field direction. The apparent anisotropy in  $I(\theta)$  can be understood from the following physical arguments. The electric field mixes into the pure  $\psi_0(2s_{1/2})$  state some of the  $\psi_0(2p_{1/2})$  and  $\psi_0(2p_{3/2})$  states, and the field perturbed  $\psi(2s_{1/2})$  becomes

$$\psi(2s_{1/2}) = \psi_0(2s_{1/2}) + a\psi_0(2p_{1/2}) + b\sqrt{2}\psi_0(2p_{3/2}). \quad (3)$$

The ratio of the mixing coefficients

$$\rho = \frac{b}{a} = \frac{E(2s_{1/2}) - E(2p_{1/2}) + i\Gamma/2}{E(2s_{1/2}) - E(2p_{3/2}) + i\Gamma/2} + O(F^2) \quad (4)$$

depends weakly on even powers of the field as indicated by the higher-order field correction terms  $O(F^2)$ . Here  $\Gamma$  is the level width of the  $2p$  states. In the limit of weak fields

$$\rho \rightarrow \rho_0 = \frac{\mathcal{L} + i\Gamma/2}{\mathcal{F} + i\Gamma/2} \quad (5)$$

where  $\mathcal{F} = E(2s_{1/2}) - E(2p_{3/2})$  is the Lamb shift minus the fine structure splitting  $\Delta_F = E(2p_{3/2}) - E(2p_{1/2})$ . The magnitude  $|\rho_0|$  is about  $-0.1$  for all hydrogenic ions.

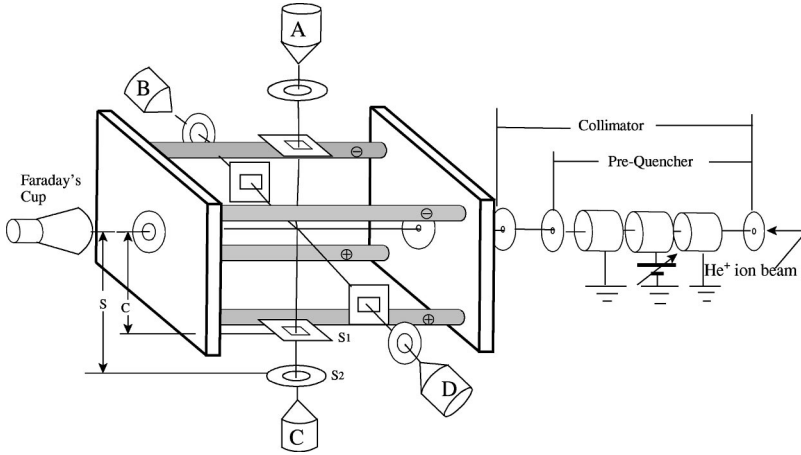


FIG. 2. Schematic diagram of the apparatus for the  $\text{He}^+$  anisotropy measurements. The four metal rods in the observation cell are 1.2700(2) cm in diameter and are supported 4.064(1) cm apart on insulators.  $S_1$  and  $S_2$  are photon collimating slits with  $c=7.117(2)$  cm and  $s=21.999(3)$  cm. Details of the schematically drawn photon detectors  $A, B, C,$  and  $D$  are shown in Fig. 3 below.

In the electric field dipole approximation, and in the limit of weak electric fields, the intensity of the radiation emitted at an angle  $\theta$  and summed over all polarization directions is

$$I(\theta) \propto 1 + \text{Re}(\rho_0)(1 - 3 \cos^2 \theta) + \frac{1}{2} |\rho_0|^2 (5 - 3 \cos^2 \theta) \quad (6)$$

(see Ref. [6]). This equation assumes that the intensities are averaged over opposite observation directions, as is done in the experiment, and it also temporarily ignores the  $M2$  transitions.

With the notation  $I(0^\circ) = I_{\parallel}$  and  $I(90^\circ) = I_{\perp}$ , the anisotropy  $R$ , defined as the relative difference in the intensities emitted parallel and perpendicular to the field,  $R = (I_{\parallel} - I_{\perp}) / (I_{\parallel} + I_{\perp})$ , becomes

$$R_0 = - \frac{3 \text{Re}(\rho_0) + \frac{3}{2} |\rho_0|^2}{2 - \text{Re}(\rho_0) + \frac{7}{2} |\rho_0|^2}. \quad (7)$$

Since  $\text{Re}(\rho_0) \sim -0.1$ , the anisotropy is about a 15% effect for all hydrogenic ions, and a measurement of  $R_0$  is equivalent to a measurement of the Lamb shift since the fine structure splitting  $\Delta_F$  is (to lowest order) a non-QED effect that is more accurately known. Equation (7) can be solved for the Lamb shift in terms of  $R_0$  and  $\Delta_F$  to obtain

$$\mathcal{L} = \frac{1}{3} \left[ \Delta_F - \sqrt{\Delta_F^2 \left( \frac{1 - 3R_0}{1 + R_0} \right) - \frac{9\Gamma^2}{4}} \right]. \quad (8)$$

Small corrections to the calculated  $R_0$  at zero field arise from field induced mixing of the  $1s$  and  $2s$  states with higher  $np$  states, relativistic corrections to the matrix elements, and magnetic quadrupole ( $M2$ ) transitions from the  $2p_{3/2}$  state to the ground state. On neglecting the level with  $\Gamma$  in Eq. (7), the fractional corrections are [3]

$$\left( \frac{\delta R}{R_0} \right)_{np} = \frac{3\mathcal{F}}{\hbar\omega} \left( \frac{1 + 2\rho_0}{2 + \rho_0} \right) (1 + R_0), \quad (9)$$

$$\left( \frac{\delta R}{R_0} \right)_{\text{rel}} = 0.0681 (Z\alpha)^2 \left( \frac{1 + 2\rho_0}{2 + \rho_0} \right) \left( \frac{1 + R_0}{1 - \rho_0} \right), \quad (10)$$

$$\left( \frac{\delta R}{R_0} \right)_{M2} = \frac{-9(Z\alpha)^2}{32} \left( \frac{(1 - \rho_0)(1 - R_0/3)}{1 + \rho_0/2} \right), \quad (11)$$

where  $\hbar\omega = E(2s_{1/2}) - E(1s_{1/2})$ . With these corrections, and corrections for finite electric field strength  $F$ , the total anisotropy becomes

$$R_T = R_0 \left[ 1 + \left( \frac{\delta R}{R_0} \right)_{np} + \left( \frac{\delta R}{R_0} \right)_{\text{rel}} + \left( \frac{\delta R}{R_0} \right)_{\text{rel}} \right] + R^{(2)} F^2 + R^{(4)} F^4 + \dots \quad (12)$$

From a measurement of  $R_T$  at the known field  $F$ , this equation can be solved for  $R_0$  and the Lamb shift calculated from Eq. (8), using the input data of Table II.

## B. Relation between polarization and anisotropy

Neglecting retardation effects, the electric dipole transition operator is simply  $-\hat{e} \cdot \mathbf{r}$ , where  $\hat{e}$  is the photon polarization vector, independent of the direction of propagation. There is then a simple geometrical connection between the anisotropy and the polarization of the emitted radiation, as shown in Fig. 1(c). If the radiating system is located at the origin and the quenching electric field  $\mathbf{F}$  is directed along the  $z$  axis, then the total radiation emitted parallel to the  $z$  axis is  $I_{\parallel} = I(\hat{e}_x) + I(\hat{e}_y)$ . But because the  $z$  axis is a symmetry axis,  $I(\hat{e}_x) = I(\hat{e}_y)$ , and thus the radiation traveling parallel to the field direction is unpolarized. However, the total radiation emitted perpendicular to the field (say, in the  $x$  direction) is  $I_{\perp} = I(\hat{e}_y) + I(\hat{e}_z)$ . The polarization for  $I_{\perp}$  is thus

$$P \equiv \frac{I(\hat{e}_y) - I(\hat{e}_z)}{I(\hat{e}_y) + I(\hat{e}_z)} = \frac{2R}{1 - R}. \quad (13)$$

For  $\text{He}^+$ ,  $R \approx 0.118$ , and so the perpendicular radiation is 27% polarized. It is apparent that in a measurement of  $R$  the photon detection system must have the same photoelectric sensitivity for detection of the unpolarized  $I_{\parallel}$  radiation as for the polarized  $I_{\perp}$  radiation. This requires that the photon detectors be insensitive to the polarization of the incident Ly  $\alpha$  radiation.

#### IV. EXPERIMENT

##### A. Overall plan

The anisotropy method is illustrated in Fig. 2, where a beam of 130.0(5) keV He<sup>+</sup> ions consists mainly of ground state ions with a concentration of 1–2% of the desired metastable He<sup>+</sup>(2*s*) ions. The beam current is about 1 μA for a beam with a diameter of 0.25 cm. The beam passes through some cylindrical prequenching electrodes whose polarities are normally switched off. The prequenching electric fields are switched on only to destroy the metastable states for the purpose of determining small noise signals. After the prequenching region, the beam enters the observation region. Here it is subjected to a static electric field by supplying appropriate polarities to the cylindrical rods mounted on insulators in a quadrupole arrangement. The resulting electric field induced Ly α intensities are detected simultaneously by the photon detectors *A*, *B*, *C*, and *D*. For the case shown in the diagram where opposite polarities are applied to adjacent pairs of quadrupole rods, the *A* and *C* detectors view the radiation parallel to the field direction while the *B* and *D* detectors view the perpendicular radiation. For each measurement of the anisotropy, the roles of the detectors are interchanged by switching potentials on the rods so that the electric field rotates in steps of 90°. This allows measurements that are independent of the relative photoelectric efficiencies of the photon detectors, which thus need not be known.

##### B. Photon detection

The Ly α photons from the beam pass through a photon collimator with entrance slit *S*<sub>1</sub> and exit slit *S*<sub>2</sub> and then strike a large photosensitive surface from which the photoelectric current emitted (of the order 10<sup>-14</sup> A) is collected and directly measured with sensitive electrometers. To stop low-energy particles that are produced by the interaction of the fast beam with the remaining gas ( $P \sim 5 \times 10^{-8}$  Torr) in the observation region from striking the photosensitive surfaces, the circular exit slit *S*<sub>2</sub> of each photon collimator is covered with a self-supporting thin (~800 Å) Al film that is about 60% transparent to the 300 Å Ly α radiation. In addition, an axial magnetic field of 20.0(2) G over the observation region confines low-energy electrons traveling with the beam, and generated by the beam, to the beam region in the presence of the quenching field.

In our previous He<sup>+</sup> experiment, the photosensitive surfaces consisted of cones, as shown in Fig. 2, with cone angles of 96°. These were mounted such that the tip of a cone viewed the He<sup>+</sup>(2*s*) beam along the central photon collimator axis, oriented perpendicular to the beam. From symmetry arguments it follows that such a cone possesses no polarization sensitivity of photoelectric emission for photons that strike the cone for very small angular ranges about the photon collimator axis. However, we recently found that, for finite viewing ranges of the beam that are still allowed by the collimator, the cones possess a small overall polarization sensitivity, contrary to our conclusions drawn from earlier tests. There we found that although the apparent Lamb shift

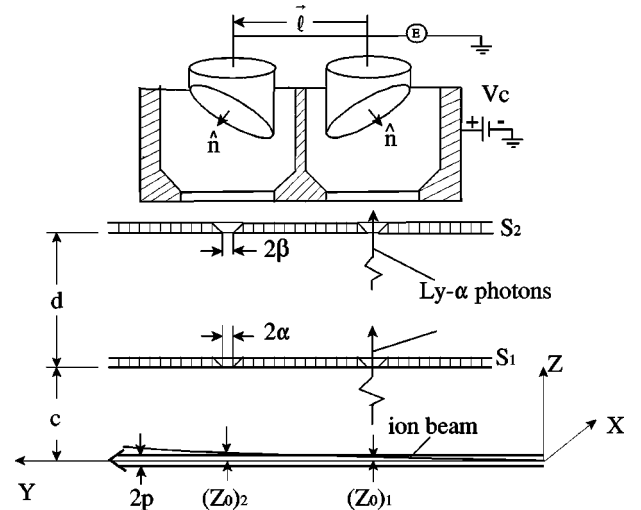


FIG. 3. Details of the photon detectors *A*, *B*, *C*, and *D* shown schematically in Fig. 2. The beam is  $2p = 0.254$  cm in diameter; the width of the rectangular slits *S*<sub>1</sub> is  $2\alpha = 1.245$  cm; the diameter of the circular slits *S*<sub>2</sub> is  $2\beta = 1.270$  cm. Distances of slits *S*<sub>1</sub> and *S*<sub>2</sub> from the beam axis are  $c = 7.117$  cm and  $d = 14.883$  cm, respectively. *V*<sub>c</sub> is a 300 V collector potential for photoelectrons and *E* is an electrometer. The separation between the photosensitive surfaces is  $l = 3.048$  cm. The normal  $\hat{n}$  projects out of the page such that it makes equal angles of  $\theta = 60^\circ$  with both the  $\hat{x}$  and  $\hat{y}$  directions shown in the figure. The deflections  $(z_0)_1$  and  $(z_0)_2$  [see Eq. (22)] are due to the transverse field and are exaggerated for clarity.

depended on cone angle it was independent of cone angles in the range 75° to 120° studied at the 100 ppm precision level. It turns out that the existence of such an angular plateau does not imply the absence of an overall polarization sensitivity, and this accounts for our earlier experiment [3] which gave an apparent anisotropy that is too large.

##### C. Redesigned photon detectors

The polarization sensitivity discussed above occurs because the photoelectric yield depends on the angle  $\theta$  between the electric field vector of the incident radiation and the normal to the photosensitive surface. For example, we found that for a flat metallic surface, coated with a thin layer of MgF<sub>2</sub> to enhance the photoelectron yield by an order of magnitude, the angular dependence of the photoelectric yield for 300 Å Ly α radiation has the approximate form

$$Y(\theta) \propto 3.05 + \cos \theta \quad (14)$$

for the angular range  $\theta = 60^\circ$  to  $90^\circ$  studied.

In order to overcome this problem, we have constructed photon detectors whose overall photoelectron yield is independent of polarization of the incident radiation. Each photon detector, such as detector *A* in Fig. 2, now consists of two flat surfaces mounted in tandem, along the beam (*y*) direction as shown in Fig. 3. Each flat surface is machined onto a 2.5 cm Al cylinder making an angle of 45° with the cylinder axis. The cylinder is mounted so that its axis coincides with

the photon collimator axis. The critical parameter in achieving polarization insensitivity is not the  $45^\circ$  angle with the cylinder axis, but the angular orientation of the photosensitive flat surfaces with respect to the photon collimator axis. The normal  $\hat{\mathbf{n}}$  must make equal angles of  $\theta=60^\circ$  with both the  $\hat{\mathbf{x}}$  and  $\hat{\mathbf{y}}$  directions.

To find the angular precision with which an Al cylinder must be mounted, suppose that it is rotated about its axis by a small angle  $\delta\theta$  from its ideal position. Then the relative uncertainty in the observed anisotropy is  $\delta R/R \approx \delta\theta/(7R)$  for the angular dependence  $Y(\theta)$  in Eq. (14). For  $R \sim 0.118$  and  $\delta\theta$  equal to  $1''$ , the uncertainty in the anisotropy (and hence in the Lamb shift) is 5 ppm.

In practice, we can hold the angular tolerance to a value of at best  $\delta\theta \sim 100''$ . To overcome the resulting large error  $\delta R/R \sim 500$  ppm, a second identical cylinder is mounted in tandem with the first cylinder at a distance  $\ell = 3.048$  cm as shown in Fig. 3. After the two cylinders are rigidly mounted onto a single metal block, the two flat surfaces are machined with the aid of a precision rotatable table such that the two normals have the same  $x$  components, but opposite  $y$  components, and such that the angle between the two normals is correct to within  $1''$ . The two photosensitive surfaces so machined are then polished nearly flat and vacuum coated with a thin layer of  $\text{MgF}_2$  to increase the photoyield to the 20% level. The whole unit is then positioned with the vector  $\ell$  between the cylinders (see Fig. 3) parallel to the beam direction with an angular tolerance of about  $200''$ .

The photoelectric currents emitted by the two surfaces are combined and detected as a single photocurrent. Thus, because the angular uncertainty in the orientation of  $\ell$  results in errors in the anisotropy for the two surfaces of opposite sign, the combined photocurrent is insensitive to polarization, even for the finite viewing ranges of the beam axis allowed by the photon collimator.

Second-order errors are introduced by the depletion of the Ly  $\alpha$  signal along the metastable beam, which results in a higher photon signal striking the upstream than the downstream surfaces. To eliminate the resulting error, the normals to the surface of the  $C$  detector, viewing the beam from below (see Fig. 2), have the same  $x$  components, but opposite  $y$  components, from the corresponding normals to the surfaces of the  $A$  detector.

Cancellation of higher-order effects, such as those introduced by slightly different photosensitivities of the surfaces, requires an averaging of data over interchanges of detectors  $A$  and  $C$ , and  $B$  and  $D$ , together with a  $180^\circ$  rotation about the collimator axis for each detection system. Furthermore, since it cannot be ruled out that the thin Al films covering the exit slit  $S_2$  of the photon collimators introduce a residual polarization sensitivity for Ly  $\alpha$  transmission, the data are also averaged over two film orientations by rotating them through  $90^\circ$  and interchanging the films for the upstream and downstream detectors.

#### D. Data collection

To eliminate effects from ion beam current fluctuations, the photoelectron current for each detector system is normal-

ized to the beam current and then averaged for 60 s. Subtracted from the signal is the small noise current (0.3%) which we define as the signal that still persists when the  $\text{He}^+(2s)$  state is removed from the beam by prequenching, to form ground state  $\text{He}^+(1s)$  ions. The quantity directly measured is the intensity ratio  $r = I_{\parallel}/I_{\perp}$ , which is related to the anisotropy by  $R = (r-1)/(r+1)$ .

The need to measure the relative photoelectric efficiencies of the detectors was avoided by measuring  $r$  for all possible  $90^\circ$  rotations of the electric field direction in Fig. 2. For example, let  $\theta$  be the angle between  $\mathbf{F}$  and the  $CA$  axis. Then for any pair of adjacent detectors, say  $A$  and  $B$ , the four current ratios  $r(\theta)$  are

$$r(0) = \frac{A(0)}{B(0)}, \quad r(\frac{1}{2}\pi) = \frac{B(\frac{1}{2}\pi)}{A(\frac{1}{2}\pi)}, \quad (15a)$$

$$r(\pi) = \frac{A(\pi)}{B(\pi)}, \quad r(\frac{3}{2}\pi) = \frac{B(\frac{3}{2}\pi)}{A(\frac{3}{2}\pi)}, \quad (15b)$$

where  $A(\theta)$  and  $B(\theta)$  are simultaneously measured time averaged photoelectron currents. Then the combination

$$r_{AB} = \frac{1}{2} \left( \sqrt{r(0)r(\frac{1}{2}\pi)} + \sqrt{r(\pi)r(\frac{3}{2}\pi)} \right) \quad (16)$$

is independent of the photoelectric efficiency. Furthermore, the average

$$r = \frac{1}{4} (r_{AB} + r_{BC} + r_{CD} + r_{DA}) \quad (17)$$

over all four adjacent detector pairs does not contain a first-order correction due to transverse beam deflections (beam bending) in the quenching field. Small second-order correction are discussed in Sec. IV B. Thus a single measurement for  $r$  consists of measuring the time-averaged signal currents simultaneously for each detector and for each of the four electric field directions, followed by the corresponding noise measurements.

## V. RESULTS

### A. Uncorrected data

For a given orientation of the thin Al films on the exit slits of the photon collimator we carried out the following four series of measurements of  $r$ , each to the same level of precision and all at the same quenching field  $F = 632.03(22)$  V/cm: (1) an initial run with the detectors mounted as described in Sec. IV C, (2) a run with detector interchanges  $A \rightleftharpoons B$  and  $C \rightleftharpoons D$ , together with a  $180^\circ$  rotation about their photon collimator axes, (3) a run with each detector system rotated by  $180^\circ$ , and (4) a run with detector interchanges  $A \rightleftharpoons C$  and  $B \rightleftharpoons D$ , together with a  $180^\circ$  rotation of each system. These four measurements were then repeated after a  $90^\circ$  rotation and interchange of the thin Al films as discussed in Sec. III C. The average anisotropy ratio for a set of these four measurements is insensitive to small variations

TABLE III. Observed anisotropy ratios  $r$  at  $F=632.03$  V/cm.

Measuring series	Thin Al film orientation	
	Unrotated	Rotated by $\pi/2$
I	1.267 624 59(999)	1.267 613 47(915)
II	1.267 624 84(1055)	1.267 608 09(906)
III	1.267 628 21(1009)	1.267 631 47(939)
IV	1.267 623 65(987)	1.267 649 72(1050)
Average	1.267 625 32(506)	1.267 625 69(477)

in the angular alignment of  $\ell$  in Fig. 3, and also insensitive to small differences in the photoelectric efficiencies.

The results are summarized in Table III, where each value listed is the average of nine runs, with each run consisting of about 30 individual measurements. It is satisfying that there are no large deviations from the average for all the eight measurements and that the average  $r$  value for the two film orientations is the same. The final anisotropy ratio, averaged over the two film orientations, is  $r=1.267\,625\,50(348)$ , corresponding to an uncorrected experimental anisotropy  $R_{\text{exp}}=0.118\,020\,15(135)$ .

### B. Systematic corrections

The above experimental value for the anisotropy requires several corrections. There is a correction for a small isotropic component of the signal resulting from  $2E1$  two-photon transitions to the ground state, a correction for averaging the signal over the finite solid angle of the detection, a correction for beam bending, and a relativistic angular shift. These are now discussed in the following subsections.

#### 1. Two-photon background

The quenching signal contains a small isotropic background from the spontaneous  $2E1$  decay [27] of the  $2s_{1/2}$  state, which much be subtracted. For each detector the apparent observed anisotropy in the presence of the  $2E1$  two-photon signal  $I(2E1)$  is

$$R_a = \frac{I_{\parallel} - I_{\perp}}{I_{\parallel} + I_{\perp} + 2I(2E1)}. \quad (18)$$

The resulting relative error in  $R$  becomes

TABLE IV.  $I_0(2E1)$  at  $F=0$  and  $I_{\parallel}$  at  $F=632$  V/cm for the four detectors.

Intensity	Detector			
	A	B	C	D
$I_0(2E1)^a$	$1.102(116) \times 10^{-5}$	$1.618(224) \times 10^{-5}$	$1.030(86) \times 10^{-5}$	$1.200(308) \times 10^{-5}$
$I_{\parallel}^b$	0.728	0.700	0.687	0.712

<sup>a</sup>The large differences in the statistical error for the four detector systems arise from small differences in the rms noise currents ( $\sim 10^{-17}$  A) of the electrometers.

<sup>b</sup>The variation in  $I_{\parallel}$  for the various detectors reflects the difference of Ly  $\alpha$  transmission through the Al films.

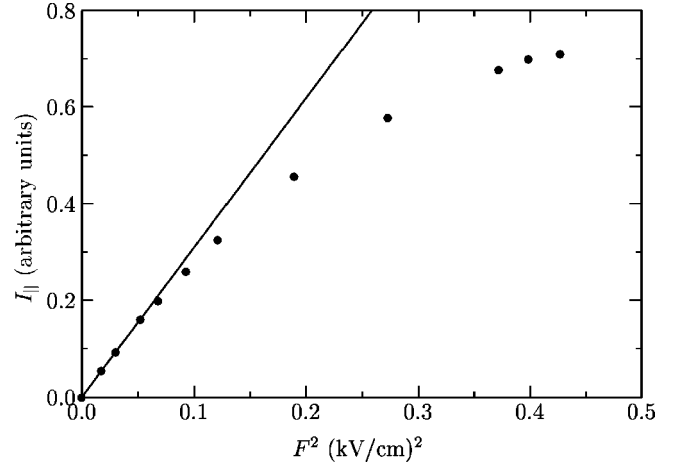


FIG. 4. The field dependence of  $I_{\parallel}$  for detection system B. The straight line is the tangent to the experimental points at zero field.

$$\frac{\delta R}{R} = (1+R) \frac{I(2E1)}{I_{\parallel}}, \quad (19)$$

where  $\delta R = R - R_a$ , and the quantity  $I(2E1)/I_{\parallel}$  represents the response of the detector to the broad two-photon continuum ( $0 \leq \nu \leq \nu_{\text{Ly } \alpha}$ ) relative to the response for the  $I_{\parallel}$  Ly  $\alpha$  radiation. To calculate this requires a knowledge of the photoelectric efficiency over the entire frequency spectrum. Since for our detection systems this frequency dependence cannot be inferred from the literature (see Ref. [3]) with sufficient accuracy, we have instead measured the  $I(2E1)/I_{\parallel}$  ratio to the 10% precision level, as follows.

The principle of the measurement is to calculate  $I(2E1)$  from  $I(2E1) = fI_0(2E1)$ , where  $I_0(2E1)$  is the two-photon signal at zero field strength, and the factor  $f$  corrects for the depletion of metastables along the beam at our normal quenching field of  $F=632$  V/cm. The first row of Table IV shows the values of  $I_0(2E1)$  for each of the detectors, averaged over 550 individual measurements. Normalization of the photocurrents to the beam current makes these numbers dimensionless. The  $I_0(2E1)$  signals are small compared to the normal  $I_{\parallel}$  signals, which are listed in the second row. The  $I_0(2E1)$  signals are the same within statistical fluctuations for all detectors and their average, averaged over the four detectors, is  $I_0(2E1) = 1.237(114) \times 10^{-5}$ .

Next the depletion fraction  $f$  of metastables in the beam was measured from the variation of  $I_{\parallel}$  with field strength, as shown in Fig. 4. The straight line represents the quadratic

dependence of  $I_{\parallel}$  on  $F$  at low field strengths due to the field induced decay rate [27]

$$\gamma(F) = (eF)^2 \gamma_{2p} \left( \frac{|\langle 2s_{1/2} | z | 2p_{1/2} \rangle|^2}{\mathcal{L}^2 + \Gamma^2/4} + \frac{|\langle 2s_{1/2} | z | 2p_{3/2} \rangle|^2}{\mathcal{L}^2 + \Gamma^2/4} \right), \quad (20)$$

and  $\gamma_{2p} = 2\pi\Gamma$ . The departure of the measured points from the straight line corresponds to a depletion fraction of  $f = 0.577$  at  $F = 632$  V/cm, and so the corrected two-photon background signal is  $I(2E1) = 0.714(66) \times 10^{-5}$ . Combining this with the average  $I_{\parallel}$  signal for the four detectors of  $I_{\parallel} = 0.707$  (see Table IV), the final correction is  $\delta R = 1.33(12) \times 10^{-6}$ . This is in approximate agreement with our earlier estimate  $\delta R = 1.64(16) \times 10^{-6}$  [3].

Finally, care must be taken during the measurement of  $I_0(2E1)$  to reduce stray magnetic fields perpendicular to the beam direction to the 0.1 G level because these fields produce a  $\mathbf{v} \times \mathbf{B}$  motional electric field. At our beam velocity  $v/c = 8.35 \times 10^{-3}$ , a stray field of 0.1 G produces a motional electric field of 0.25 V/cm. The resulting Ly quench radiation intensity of  $I_{\text{stray}} \sim 2 \times 10^{-7}$ , as derived from the data for Fig. 4, mimics the spontaneous  $2E1$  background. It is satisfying that the stray signal lies nearly two orders of magnitude below  $I_0(2E1) = 1.237 \times 10^{-5}$ .

## 2. Finite solid angle and beam bending

The correction for finite solid angle of observation takes into account the finite sizes of the photon collimator slits, along with effects from beam bending and the depletion of the concentration of the metastable ions along the beam. Once the corrections have been obtained for a single detector, they must be averaged over the detector pairs shown in Fig. 3, with weighting factors  $w_1$  and  $w_2$  equal to the relative radiation intensities.

The radiation intensity decays exponentially along the beam as  $I(y) = I_0 e^{-\gamma_y y}$ . The beam has a parabolic trajectory

$$z = z_0 + \lambda(y - y_0) + \mu(y - y_0)^2 \quad (21)$$

in the field, where  $y_0 = 7.62$  cm is the center position of the quenching cell from its entrance slit at  $y = 0$ , and  $z_0$  is the beam deflection. The velocity ratio  $\lambda = v_z/v_y$  in the  $z$  and  $y$  directions must be evaluated at the center of the detector viewing region. Finally  $\mu = F/V_a$ , where  $V_a = 130$  kV is the accelerating potential. In terms of these constants and the ones shown in Figs. 2 and 3, the observed anisotropy  $R$  is related to the solid angle corrected anisotropy  $R_c$  by

$$\begin{aligned} \frac{R}{R_c} &= 1 - \frac{p^2}{2s^2} - (1 - R_c) \frac{t^2}{s^2} \left( \frac{\alpha^2}{3} + \frac{\beta^2}{4} \right) - \frac{\beta^2}{2s^2} + \frac{\tilde{z}_0^2}{R_c s^2} \\ &\times \left[ \frac{9}{4} (1 - R_c^2) - R_c \right] - \frac{\tilde{z}_0^2}{R_c s^2} (1 - R_c^2), \end{aligned} \quad (22)$$

where

TABLE V. Parameters for calculating the solid angle and beam bending corrections of Eq. (23).  $\delta R/R$  is the relative error in  $R$  corresponding to the uncertainty in each parameter.

Parameter	Value	$\delta R/R$ (ppm)
$\alpha$	0.622 3(13) cm	2.15
$\beta$	0.635 0(13) cm	3.36
$c$	7.117 1(25) cm	0.09
$d$	14.882 6(25) cm	0.39
$p$	0.127(9) cm	2.45
$\mu$	$12.155(103) \times 10^{-4}$ cm <sup>-1</sup>	0.00
$\lambda_1$	0.012 11(93)	0.05
$\lambda_2$	0.019 52(155)	0.10
$(z_0)_1$	0.031 31(25) cm	0.23
$(z_0)_2$	0.079 52(64) cm	1.30
$w_1$	0.574 59(34)	0.00
$w_2$	0.425 41(34)	0.00
$\gamma_y$	0.100 200(10) cm <sup>-1</sup>	0.00

$$\tilde{z}_0^2 = z_0^2 + [\lambda^2 + 2(\mu - \lambda \gamma_y) z_0] \left[ \frac{\alpha^2 t^2}{3} + \frac{\beta^2 (1-t)^2}{4} \right],$$

$$\tilde{z}_0^2 = z_0^2 + \frac{1}{2} [\lambda^2 + 2(\mu - \lambda \gamma_y) z_0] \left[ \alpha^2 t^2 + \frac{\beta^2 (3t^2 - 6t + 2)}{4} \right],$$

and  $t = s/d$ .

Equation (22) assumes that the signals from opposite detectors are averaged so that first-order corrections from beam bending cancel. The input parameters for Eq. (22) and their uncertainties, along with the resulting relative errors  $\delta R/R$  in the anisotropy, are listed in Table V. The subscripts 1 and 2 on the parameters refer to the upstream and downstream detectors as shown in Fig. 3. The weighted  $R/R_c$  value for a detection pair  $R/R_c = 0.998\,715\,7(49)$  corresponds to the correction  $\delta R = R_c - R$  equal to  $\delta R = 0.000\,151\,766(590)$ .

## 3. Relativistic angular shift

The observed intensity  $I_{\parallel}$  emitted parallel to  $F$  in the laboratory frame by the moving ions corresponds to emission at a small angle  $\theta = v/c$  to  $F$ . The resulting correction to the anisotropy is

$$\frac{\delta R}{R_c} = (1 - R_c) \left( \frac{v}{c} \right)^2. \quad (23)$$

## 4. Zeeman splitting and $\mathbf{v} \times \mathbf{B}$ fields

The Zeeman splitting for the  $n = 2$  manifold of states in an axial magnetic field  $\mathbf{B}$  produces in second order an enhanced Stark coupling between the  $2s_{1/2}$  and  $2p_{1/2}$  sublevels whereby the anisotropy is decreased. For our field of  $B = 20.0(2)$  G, the correction to  $R$  is  $\delta R = 0.000\,000\,680(60)$ , as obtained from a detailed numerical integration of the time-dependent Schrödinger equation for the  $\text{He}^+$  ions as they pass through the fringing field region and into the main quenching field. The Zeeman splitting also

TABLE VI. Systematic corrections to obtain the zeroth-order anisotropy  $R_0$ .

Quantity	Value
Measured anisotropy	0.118 020 15(135)
Detector nonlinearity	0.000 000 00(35)
Residual polarization sensitivity of detectors	0.000 000 00(50)
2E1 two-photon decay	0.000 001 33(12)
Finite solid angle of detectors and deflection of ion beams	0.000 151 77(57)
Relativistic angular shift	0.000 007 26(6)
20.0 G Zeeman splitting	0.000 000 68(1)
$\mathbf{v} \times \mathbf{B}$ electric field	0.000 000 36(4)
$R^{(2)}F^2 + R^{(4)}F^4$	-0.000 232 96(25)
$R_0(\delta R/R_0)_{np}$	0.000 002 80
$R_0(\delta R/R_0)_{rel}$	-0.000 000 76
$R_0(\delta R/R_0)_{M2}$	0.000 007 71
$R_0$ (sum of above)	0.117 958 34(162)
$\mathcal{L}$ from Eq. (8)	14 041.13(17) MHz

produces a slight time dependence in  $R$  as different magnetic substates depopulate at different rates.

The axial  $\mathbf{B}$  field produces a further correction. As the ion traverses the quenching field it progressively acquires a velocity component  $v_z = \lambda v_y$  in the  $z$  direction. The resulting motional  $\mathbf{v} \times \mathbf{B}$  electric field is perpendicular to  $\mathbf{F}$  and their vector sum produces a net effective quenching field that is rotated through a small angle  $\theta = V_B/cF$ . The resulting correction to the anisotropy is

$$\frac{\delta R}{R_c} = 2 \left( \frac{v_z B}{cF} \right)^2. \quad (24)$$

This must be evaluated separately for the upstream and downstream detectors to find the weighted average with the weight factors  $w_1$  and  $w_2$  listed in Table V.

### 5. Stray Field Effects

Stray electric and/or magnetic fields could in principle introduce further systematic errors. For example, a stray magnetic field  $\mathbf{B}$  perpendicular to the beam direction in the observation cell would result in a motional  $\mathbf{v} \times \mathbf{B}$  electric field that is superposed on the applied electric quenching field  $\mathbf{F}$ . To study the implications of this, assume for example that there exists a small  $\mathbf{B}$  field directed along the  $z$  direction in Fig. 3, so that the motional field points in the  $x$  direction. This must be added vectorially to the main quenching field  $\mathbf{F}$ , which points in the  $\pm z$  directions or  $\pm x$  directions as the field is progressively rotated in steps of  $90^\circ$ .

There are two cases to be considered. If  $\mathbf{F}$  points in the  $x$  direction, the direction of the resultant quenching field is not affected, but its magnitude changes by  $\pm vB$ . The linear correction cancels from the field-reversed average photon signals (which are proportional to  $F^2$ ), leaving a quadratic fractional correction of  $\delta^2 = (vB/F)^2$ . If  $\mathbf{F}$  points in the  $z$  direction, the total quenching field will be rotated through a small angle  $\delta = vB/F$ , and its strength increased by the fac-

TABLE VII. Comparison of experiment and theory for the He<sup>+</sup> Lamb shift, in units of MHz.

Experiment	Theory
14 041.13 ± 0.17 <sup>a</sup>	14 041.18 ± 0.13 [ $r_{rms} = 1.673(1)$ fm]
14 042.0 ± 1.2 <sup>b</sup>	14 041.19 ± 0.18 [ $r_{rms} = 1.674(12)$ fm]
14 046.2 ± 1.2 <sup>c</sup>	
14 040.2 ± 1.8 <sup>d</sup>	

<sup>a</sup>Present work.

<sup>b</sup>Reference [29].

<sup>c</sup>Reference [28].

<sup>d</sup>Reference [30].

tor  $(1 + \delta^2)^{1/2}$ . Thus the effective averaged value of  $F^2$  increases by the same factor of  $(1 + \delta^2)$  in both cases. Since  $R$  is independent of  $F$  in the limit of weak fields, the correction is negligible. What remains is the expression

$$R_a = \frac{I(\delta) - I(\pi/2 + \delta)}{I(\delta) + I(\pi/2 + \delta)} \quad (25)$$

for the apparent anisotropy when  $\mathbf{F}$  points in the  $z$  direction, where, from Eqs. (6) and (7),

$$I(\theta) = 1 + \frac{2R_0}{1 - R_0} \cos^2 \theta, \quad (26)$$

normalized to unity for  $\theta = \pi/2$ . There is no rotational correction (for the assumed stray field) when  $\mathbf{F}$  points in the  $x$  direction. On expanding in powers of  $\delta^2$  and averaging over the two cases, the apparent anisotropy is

$$R_a = R_0 [1 - \delta^2 + O(\delta^4)]. \quad (27)$$

During the experiment, stray magnetic fields perpendicular to the beam were cancelled by Helmholtz coils to  $\pm 0.2$  G or less. Thus at our beam velocity  $v/c \approx 8.35 \times 10^{-3}$  and quenching field  $F = 632$  v/cm,  $\delta^2 \approx 0.62 \times 10^{-6}$ , which is negligibly small.

Similarly the correction resulting from stray electric fields can be ignored. The reason is that at our operating field, the applied potentials on the quadrupole rods are  $\pm 1450$  V. Such high potentials ensure that uncertainties in the direction of the net electric quenching field introduced by contact potentials ( $\sim 1$  V) are negligibly small.

### C. Summary of corrections and Lamb shift

The numerical values for the various corrections for the input data of Tables II and V are summarized in Table VI, together with the experimental anisotropy  $R_{exp}$  at  $F = 632.03(22)$  V/cm.

A check was made for the relatively large correction  $R^{(2)}F^2 + R^{(4)}F^4$  for finite quenching fields and for the correction for finite solid angle of detection described by Eq. (22). The field correction was tested in an independent series of measurements at  $F = 632$  V/cm and  $F = 479.5$  V/cm. At these fields the anisotropy corrections are, respectively,  $\delta R = 0.000 239 59(250)$  and  $\delta R = 0.000 134 216(190)$ . Al-

though these field corrections differ by nearly a factor of 2, we obtained within 40 ppm the same  $R_0$  values, which were each measured to a precision of 55 ppm. This confirms that our experiment is virtually free from field-dependent systematic corrections, other than that already contained in the  $R^{(2)}F^2 + R^{(4)}F^4$  term.

## VI. COMPARISON WITH THEORY

From Table VI, the final corrected anisotropy for a hypothetical nonrelativistic three-level hydrogen atom is  $R_0 = 0.117\,958\,34(162)$ . This is the quantity, together with the calculated fine structure splitting  $\Delta_F$ , that is to be substituted into Eq. (8) to determine the Lamb shift. The result is  $\mathcal{L} = 14\,041.13 \pm 0.17$  MHz, in excellent agreement with the theoretical value  $14\,041.18(13)$  from Table I (or  $14\,041.19 \pm 0.18$  MHz if the less accurate electron scattering value of  $r_{\text{rms}}$  is used). In either case, the experimental uncertainty, and the difference between theory and experiment, is an order of magnitude less than the two-loop binding correction of  $-1.339$  MHz.

## VII. DISCUSSION

Our present experimental value for the Lamb shift lies six standard deviations below our 1991 value of  $14\,042.52 \pm 16$  MHz [3]. The difference is entirely accounted for by the elimination of residual polarization sensitivity in the photon detection system. All other aspects of the apparatus are identical to our previous work on both hydrogen [4] and helium [3]. The good agreement obtained with other measurements and with theory for hydrogen at the same level of accuracy gives confidence that systematic effects are under good control.

We compare in Table VII our current measurement with past measurements and theory. Our measurement is in good agreement with the currently best microwave resonance value of  $14\,042.0 \pm 1.2$  MHz, but is an order of magnitude more accurate. It is satisfying that the two very different methods for measuring the Lamb shift yield the same result. Only the older measurement of Narasimham and Strombotne [28] ( $14\,046.2 \pm 1.2$  MHz) is in disagreement with the others.

Not included in Table VII are two earlier less accurate

measurements of the Lamb shift by the anisotropy method [8,9]. These used the same cone-based detector system as in the 1991 measurement [3], and so they suffered from the same systematic error due to polarization sensitivity. The difference between the present measurement and the 1991 measurement is  $1.39 \pm 0.24$  MHz. If this downward polarization correction is applied to the two earlier measurements, then the results are  $14040.5 \pm 1.5$  MHz [8] and  $14040.83 \pm 0.35$  MHz [9], in reasonable agreement with the present work.

Our current anisotropy measurement for the Lamb shift in  $\text{He}^+$  removes the only significant disagreement between theory and experiment for Lamb shifts in hydrogenic systems. The good agreement with theory in a case where the nuclear radius uncertainty is not a significant consideration suggests that Lamb shift measurements in hydrogen could be interpreted as a measure of the proton radius, rather than as a test of QED.

The main limitation on accuracy after several months of data collection is still the statistical uncertainty in the measured anisotropy as shown in Table VI. A further factor of 2 reduction in the uncertainty could be obtained before machining tolerances and geometrical uncertainties became a significant factor. At this level, the accuracy would be  $\pm 0.085$  MHz (6 ppm), which would match or exceed the best measurements in hydrogen.

The only anisotropy measurement to date for a heavier hydrogenic ion is the  $\text{O}^{7+}$  Lamb shift of  $2192 \pm 15$  GHz obtained by Curnutte *et al.* [31], using an electrostatic quenching field. There is considerable scope for further measurements of improved accuracy in the heavier hydrogenic ions, and in particular for the use of a transverse magnetic field to generate a  $\mathbf{v} \times \mathbf{B}$  electric quenching field of sufficient strength. This strategy would avoid the background noise resulting from the acceleration of charged particles into the photon detectors by a strong electrostatic quenching field.

## ACKNOWLEDGMENTS

The authors are grateful to Micha Eides and Howard Grotch for helpful correspondence concerning their tabulation of theoretical contribution to the Lamb shift. Research support by the Natural Sciences Engineering Research Council of Canada is gratefully acknowledged.

- 
- [1] K. Pachucki, Phys. Rev. Lett. **72**, 3154 (1994).  
 [2] M. Eides and V. Shelyuto, Phys. Rev. A **52**, 954 (1995), and earlier references therein.  
 [3] A. van Wijngaarden, J. Kwela, and G.W.F. Drake, Phys. Rev. A **43**, 3325 (1991).  
 [4] A. van Wijngaarden, F. Holuj, and G.W.F. Drake, Can. J. Phys. **76**, 95 (1998).  
 [5] A. van Wijngaarden, G.W.F. Drake, and P.S. Farago, Phys. Rev. Lett. **33**, 4 (1974).  
 [6] A. van Wijngaarden and G.W.F. Drake, Phys. Rev. A **17**, 1366 (1978).  
 [7] G.W.F. Drake, S.P. Goldman, and A. van Wijngaarden, Phys. Rev. A **20**, 1299 (1979).  
 [8] J. Patel, A. van Wijngaarden, and G.W.F. Drake, Phys. Rev. A **36**, 5130 (1987).  
 [9] G.W.F. Drake, J. Patel, and A. van Wijngaarden, Phys. Rev. Lett. **60**, 1002 (1988).  
 [10] G.W.F. Drake and R.B. Grimley, Phys. Rev. A **8**, 157 (1973).  
 [11] G.W.F. Drake, J. Kwela, and A. van Wijngaarden, Phys. Rev. A **46**, 113 (1992).  
 [12] A. van Wijngaarden, J. Patel, and G.W.F. Drake, Phys. Rev. A **33**, 312 (1986).  
 [13] G.W.F. Drake and R.A. Swainson, Phys. Rev. A **41**, 1243 (1990).

- [14] M. Eides, H. Grotch, and V.A. Shelyuto, Phys. Rep. (to be published).
- [15] P.J. Mohr and B.N. Taylor, J. Phys. Chem. Ref. Data **28**, 1713 (1999).
- [16] K. Pachucki, Phys. Rev. A **46**, 648 (1992); Ann. Phys. (N.Y.) **236**, 1 (1993).
- [17] U. Jentschura and K. Pachucki, Phys. Rev. A **54**, 1853 (1996).
- [18] P.J. Mohr, Phys. Rev. A **46**, 4421 (1992).
- [19] P.J. Mohr, in *Atomic, Molecular, and Optical Physics Handbook*, edited by G.W.F. Drake (AIP, New York, 1996), p. 345, Tables 28.2 and 28.4.
- [20] E. Borie and G.A. Rinker, Phys. Rev. A **18**, 324 (1978).
- [21] J.S. Cohen, Phys. Rev. A **25**, 1791 (1982).
- [22] H.P. von Arb *et al.*, Phys. Lett. **136B**, 232 (1984).
- [23] M. Eckhause *et al.*, Phys. Rev. A **33**, 1743 (1986).
- [24] L. Bracci and E. Zavattini, Phys. Rev. A **41**, 2352 (1990).
- [25] I. Sick, J.S. McCarthy, and R.R. Whitney, Phys. Lett. **64B**, 33 (1976).
- [26] G.W.F. Drake, in *Spectrum of Atomic Hydrogen: Advances*, edited by G.W. Series (World Scientific, Singapore, 1988).
- [27] G.W.F. Drake, Phys. Rev. A **34**, 2871 (1986).
- [28] M. Narasimham and R. Strombotne, Phys. Rev. A **4**, 14 (1971).
- [29] M.S. Dewey and R.W. Dunford, Phys. Rev. Lett. **60**, 2014 (1988).
- [30] E. Lipworth and R. Novick, Phys. Rev. **108**, 1434 (1957).
- [31] B. Curnutte, C.L. Cocke, and R.d. DuBois, Nucl. Instrum. Methods **202**, 119 (1981).